Regional Soil Moisture Biases and Their Influence on WRF Model Temperature Forecasts over the Intermountain West

JEFFREY D. MASSEY AND W. JAMES STEENBURGH

Department of Atmospheric Sciences, University of Utah, Salt Lake City, Utah

JASON C. KNIEVEL AND WILLIAM Y. Y. CHENG

National Center for Atmospheric Research, Boulder, Colorado*

(Manuscript received 10 June 2015, in final form 11 December 2015)

ABSTRACT

Operational Weather Research and Forecasting (WRF) Model forecasts run over Dugway Proving Ground (DPG) in northwest Utah, produced by the U.S. Army Test and Evaluation Command Four-Dimensional Weather System (4DWX), underpredict the amplitude of the diurnal temperature cycle during September and October. Mean afternoon [2000 UTC (1300 LST)] and early morning [1100 UTC (0400 LST)] 2-m temperature bias errors evaluated against 195 surface stations using 6- and 12-h forecasts are –1.37° and 1.66°C, respectively. Bias errors relative to soundings and 4DWX-DPG analyses illustrate that the afternoon cold bias extends from the surface to above the top of the planetary boundary layer, whereas the early morning warm bias develops in the lowest model levels and is confined to valleys and basins. These biases are largest during mostly clear conditions and are caused primarily by a regional overestimation of near-surface soil moisture in operational land surface analyses, which do not currently assimilate in situ soil moisture observations. Bias correction of these soil moisture analyses using data from 42 North American Soil Moisture Database stations throughout the Intermountain West reduces both the afternoon and early morning bias errors and improves forecasts of upper-level temperature and stability. These results illustrate that the assimilation of in situ and remotely sensed soil moisture observations, including those from the recently launched NASA Soil Moisture Active Passive (SMAP) mission, have the potential to greatly improve land surface analyses and near-surface temperature forecasts over arid regions.

1. Introduction

Accurate temperature forecasts by numerical weather prediction (NWP) models are critical for the protection of life and property, economic and operational activities, and routine day-to-day planning. Temperature forecasts not only affect near-surface (2 m) conditions, but also atmospheric stability, planetary boundary layer (PBL) heights, near-surface winds, and precipitation type. Large systematic temperature errors from the Weather Research and Forecasting (WRF) Model are observed throughout the world including over the European Alps (García-Díez et al. 2013) and the continental United States (Wyszogrodzki et al. 2013). Over the interior western United States, several studies identify an underprediction of the 2-m diurnal temperature range (DTR) with a warm (i.e., positive) 2-m temperature bias at night and in the early morning and a cold (i.e., negative) 2-m temperature bias in the afternoon. These biases, which are frequently >1°C, are found for a wide range of modeling systems, resolutions, and configurations (e.g., Cheng and Steenburgh 2005; Hart et al. 2005; Zhang et al. 2013; Massey et al. 2014).

Hypothesized contributors to the DTR underprediction include inadequate vertical or horizontal resolution, near-surface turbulence flux errors, or inaccurate land surface characteristics and processes (e.g., Hanna and Yang 2001; Mass et al. 2002; Marshall et al. 2003; Cheng and Steenburgh 2005; Massey et al. 2014). Recently, Massey et al. (2014) reduced the early

* The National Center for Atmospheric Research is sponsored by the National Science Foundation.

Corresponding author address: Jeffrey D. Massey, Dept. of Atmospheric Sciences, University of Utah, Rm. 819, 135 South 1460 East, Salt Lake City, UT 84112.
E-mail: jeff.massey@utah.edu

DOI: 10.1175/WAF-D-15-0073.1

morning warm bias in WRF simulations of three fall days over northern Utah through the use of an alternate soil thermal conductivity parameterization combined with soil moisture analyses based on in situ observations. The afternoon cold bias, however, was only partially reduced in Massey et al. (2014) and remains associated with a myriad of plausible, yet untested, error sources including 1) differences between model and observation site elevations (Liu et al. 2008b; Wyszogrodzki et al. 2013), 2) radiation parameterization errors due to the absence of three-dimensional scattering in complex terrain or tuning for lower elevations (Zhong and Fast 2003; Liu et al. 2008b; Wyszogrodzki et al. 2013), 3) underprediction of thermally forced circulations due to smoother-than-real topography making the associated subsidence warming over valleys and basins less intense during the day (Liu et al. 2008b), 4) decreased solar radiation due to excessive mountain cloud development during the day (Wyszogrodzki et al. 2013), and 5) inaccurate initialization and parameterization of land surface characteristics and processes (Cheng and Steenburgh 2005; Wyszogrodzki et al. 2013). Additionally, Zhang et al. (2013) ran simulations with varying vertical resolutions, forecast initialization times, and PBL schemes to test the influence of these parameters on the daytime cold bias over Utah, but noticed little improvement.

Soil moisture is a critical parameter for NWP because of its influence on surface sensible and latent fluxes, ground heat fluxes, surface and boundary layer winds, surface and boundary layer temperatures, and moist convection (e.g., Banta and Gannon 1995; Huang et al. 1996; Sun and Bosilovich 1996; Holt et al. 2006; Trier et al. 2008; Zhou and Geerts 2013). In general, higher soil moisture results in lower daytime and higher nighttime near-surface temperatures because of reduced thermal conductivity and evapotransporation, which have a stronger influence than concomitant decreases in surface albedo. Daniels et al. (2006) identified a daytime cold bias in their WRF simulations over Owens Valley, California, which they reduced by decreasing their analyzed initial soil moisture from a mean of 0.25 to 0.09 $m^3 m^{-3}$ based on in situ soil moisture observations. Limited-area mesoscale models, like the WRF, typically obtain their soil moisture initial conditions from operational modeling systems such as the National Centers for Environmental Prediction (NCEP) Global Forecast System (GFS) or the European Centre for Medium-Range Weather Forecasts (ECMWF) Integrated Forecast System (IFS). The land surface models (LSMs) that predict the land surface state in these operational modeling systems do not currently utilize in situ soil moisture observations (Dirmeyer et al. 2002; Dee et al. 2014). Instead, the soil moisture in the GFS LSM is nudged toward a soil moisture climatology (Dee et al. 2014), whereas the IFS uses an extended Kalman filter data assimilation approach that utilizes surface temperature, relative humidity, and satellite data as proxy observations to analyze soil moisture (Albergel et al. 2012a). Although we know of no published study examining soil moisture biases in the GFS, the operational IFS and ERA interim reanalysis are known to overestimate soil moisture, especially in drier regions (Albergel et al. 2012b).

To improve global analyses of soil moisture, a number of studies have utilized near-surface soil moisture estimates from spaceborne microwave remote sensing platforms (e.g., Jackson et al. 2010; Kerr et al. 2010). Such platforms include the Soil Moisture and Ocean Salinity mission (SMOS; Kerr et al. 2010), Advanced Microwave Scanning Radiometer for Earth Observing System (AMSR–E), and the Advanced Scatterometer (ASCAT). Although satellite soil moisture retrieval algorithms have improved in recent years, their coarse spatial resolution (>10–30 km) and large discrepancies with in situ soil moisture observations currently limit their utility (Crow et al. 2010; Jackson et al. 2010; Al Bitar et al. 2012; Albergel et al. 2012a). However, the Soil Moisture Active/Passive (SMAP) mission launched in early 2015 will measure soil moisture at higher resolution (9 km) and will provide more detailed measurements (Entekhabi et al. 2010). Its utilization has the potential to greatly improve soil moisture analyses. Another approach for estimating soil moisture is to use a land data assimilation system (LDAS), but our own in-house comparison between the high-resolution LDAS (HRLDAS) soil moisture and GFS soil moisture yielded similar results.

In this paper we examine how a regional overestimation of near-surface soil moisture in operational analyses over the Intermountain West during the fall (i.e., September and October) contributes to the underprediction of the DTR in a WRF-based forecasting system over Dugway Proving Ground (DPG) in the Great Salt Lake Desert of northwest Utah (Fig. 1). In particular, we extend the work of Massey et al. (2014) by examining the causes of the daytime cold bias and identifying differences in error structure and model sensitivity compared to the morning warm bias. We use idealized WRF single-column model simulations to help quantify the significance of the soil moisture error contribution to the DTR errors. We also use retrospective WRF simulations run for the Mountain Terrain Atmospheric Modeling and Observations Program (MATERHORN) fall field campaign (Fernando et al. 2015) from 25 September to 25 October 2012 at DPG to

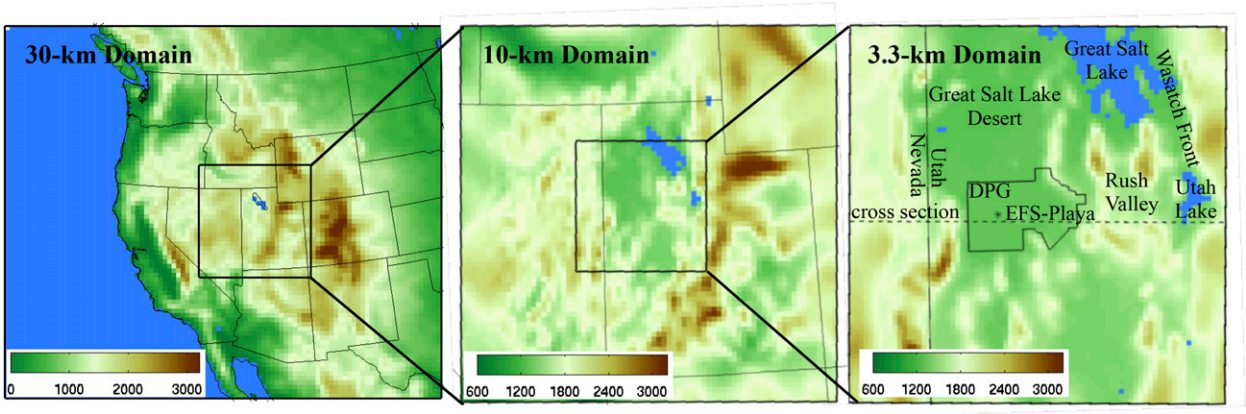

FIG. 1. The 4DWX-DPG domains with model elevation (m; shaded following color bar at bottom left) and water bodies (blue). Within the 3.3-km domain, the perimeter of DPG is outlined, the dotted line represents the location of the cross sections, and the MATERHORN EFS-Playa rawinsonde launch site is annotated.

show the temperature improvement in a fully cycled forecast system when near-surface soil moisture analyses are bias corrected and a modified soil thermal conductivity parameterization is implemented. These results suggest that efforts to incorporate soil moisture observations into land surface analyses will likely yield improved temperature forecasts over the Intermountain West and possibly other dryland regions.

2. Data and methods

a. WRF modeling

1) OPERATIONAL WRF (4DWX-DPG) FORECASTS

We identify temperature errors in 8 months of operational WRF-based forecasts produced by the U.S. Army Test and Evaluation Command Four-Dimensional Weather System (4DWX) developed by the National Center for Atmospheric Research (NCAR) and run at DPG (4DWX-DPG; Liu et al. 2008a). We concentrate on September and October of 2011, 2012, 2013, and 2014 because these months are most relevant to the MATERHORN fall 2012 field campaign. They also follow the climatologically driest and warmest months of the year (June–August) at the DPG National Weather Service Cooperative Observer site (WRCC 2015), and thus it is anticipated that soil moistures across much of the region will be at or near the annual climatological minimum. For September and October 2011, 4DWX-DPG was based on WRF v3.2, with an upgrade to WRF v3.3.1 prior to September and October 2012. The 4DWX-DPG system features 30, 10, 3.3, and 1.1-km one-way nested domains centered over DPG. For this study, we use data from only the outer three domains (Fig. 1) because temperature errors are nearly identical between the 3.3- and 1.1-km domains. The 4DWX-DPG system has 36 half-η levels, whose vertical spacing varies from ~30 m near the surface, with the lowest half-η level ~15 m AGL, to ~1250 m in the upper troposphere and lower stratosphere. The use of one-way nesting is based on its simplicity and superiority over two-way nesting in unpublished test cases.

The physics packages include the Rapid Radiative Transfer Model (RRTM) longwave radiation parameterization (Mlawer et al. 1997), Dudhia shortwave radiation parameterization (Dudhia 1989), Noah LSM (Chen and Dudhia 2001), Yonsei University PBL parameterization (YSU; Hong et al. 2006), explicit sixth-order numerical diffusion (Knievel et al. 2007), and the new Kain–Fritsch cumulus parameterization (Kain 2004). The latter was used only in the 30- and 10-km domains through 2013, then on the 3.3-km domain thereafter. Thompson et al. (2004) microphysics replaced the Lin et al. (1983) microphysics prior to September and October 2012. Rayleigh damping and an updated land cover and terrain elevation dataset based on the 33-category National Land Cover Database (NLCD; Fry et al. 2011) were added in September 2012. Playa land-use and soil texture class categories were manually added to the NLCD and WRF, respectively, to better account for the large playa in northwest Utah (i.e., Fig. 2).

The 4DWX-DPG system produces 48-h forecasts every 3 h, with nominal initialization times of 0200, 0500, 0800, 1100, 1400, 1700, 2000, and 2300 UTC. The atmospheric data assimilation stage of each forecast cycle uses Newtonian nudging for assimilating observations during the 3-h period prior to the nominal initialization time (an initialization time is conceptually equivalent

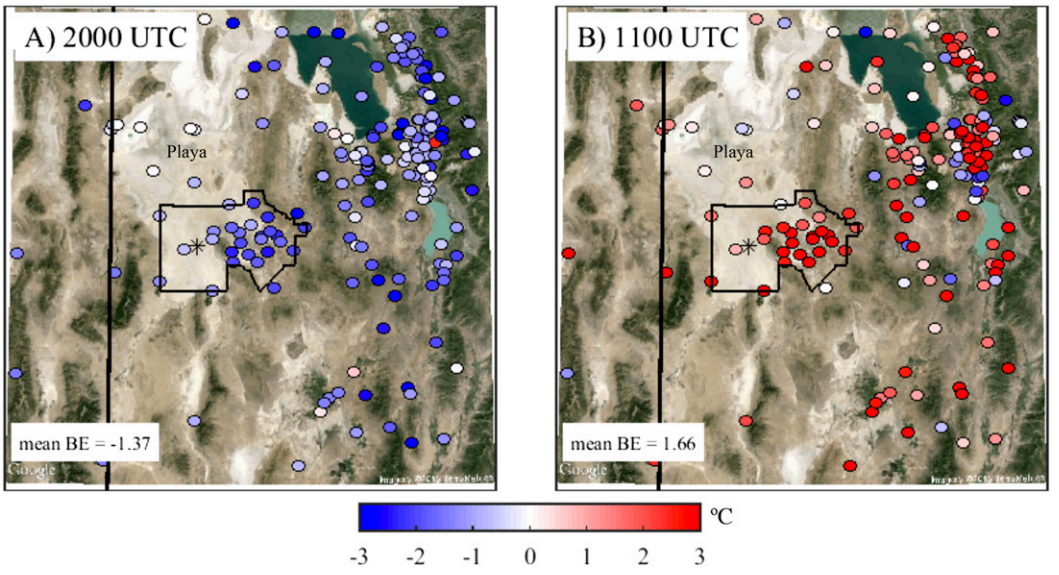

FIG. 2. Mean 4DWX-DPG 2-m temperature BEOs (°C) at Mesowest stations during the (a) afternoon (2000 UTC) and (b) early morning (1100 UTC). Overall mean BEO is annotated. (Background image provided by Google Earth; imagery also provided by TerraMetrics.) The Utah–Nevada border, DPG boundary, EFS-Playa (asterisk), and the playa are annotated for reference.

to a forecast lead time of 0 h). Observations come from aviation routine weather report (METAR) stations, rawinsondes, profilers, buoys, aircraft, satellites, and other observing platforms. In practice, some nudging is still performed during the early parts of the forecast (i.e., after 0 h) as 4DWX-DPG—following the passing of some finite time during the assimilation stage and various preprocessing steps—catches up to what is commonly called wall-clock time. The analysis at the conclusion of an assimilation stage is used to restart the assimilation of the next cycle, except for the 0500 UTC Sunday cycle when the system is ''cold started'' with an objective analysis using the 1.0° GFS analysis. At this time initial soil moisture and temperature fields are set to GFS analysis values. The initialization of soil moisture in this step is fundamental to our results, as we explain below. We use the 4DWX-DPG analyses to calculate model forecast biases given the similarity between the analyses and observations (not shown). Liu et al. (2008a) provide additional information on the 4DWX-DPG physics packages and data assimilation.

As part of the validation effort, we identify mostly clear and mostly cloudy days using a 3.3-km domain-averaged atmospheric transmittance defined as

$$\text{Transmittance} = \frac{\sum_{t=0000\ \text{LST}}^{2330\ \text{LST}} \text{SW}_{\text{sfc}}(t)}{\sum_{t=0000\ \text{LST}}^{2330\ \text{LST}} \text{SW}_{\text{toa}}(t)},$$

where $\text{SW}_{\text{sfc}}(t)$ is the domain-average downwelling shortwave radiation at the surface at time t, and $\text{SW}_{\text{toa}}(t)$ is the theoretical mean downwelling top-of-the-atmosphere shortwave radiation calculated from

$$\text{SW}_{\text{toa}}(t) = S_0 \left(\frac{a}{r}\right)^2 \sin(\varphi),$$

where S_0 is the solar constant (approximated to be 1370 W m^{-2}), a is the annual mean distance between the sun and the earth, r is the daily mean distance, and φ is the solar elevation angle calculated following Reda and Andreas (2004). Mostly clear days are defined arbitrarily as those with a transmittance > 0.65, and all other days with lower transmittance due to more clouds and aerosols are classified as mostly cloudy. Although the equation above integrates through a calendar day, the transmittance is dominated by daytime values between sunrise and sunset, the times of which vary during the verification period.

2) SINGLE-COLUMN MODEL

The WRF single-column model (SCM; Rostkier-Edelstein and Hacker 2010) is based on WRF v3.5.1 and is run to test 2-m temperature sensitivity to soil moisture, the Zilitinkevich coefficient C_{zil}, an empirical coefficient that helps control the strength of the land–atmosphere coupling), long- and shortwave radiation schemes, and PBL schemes. The SCM is run over a 3 × 3 gridpoint stencil with periodic lateral boundary conditons, no external forcing, and the same physics packages and vertical grid

spacing as in 4DWX-DPG, except in sensitivity studies involving radiation or PBL schemes. Simulations with varying C_{zil}, radiation schemes, or PBL schemes use a soil moisture of 0.235 $m^3 m^{-3}$, whereas simulations with varying soil moisture, radiation schemes, or PBL schemes use a C_{zil} of 0.518 over shrubland and 0.877 over playa.

The SCM is initialized with mean morning [1400 UTC (0700 LST)] atmospheric profiles of temperature, wind, and specific humidity, and mean soil profiles of moisture and temperature obtained from 4DWX-DPG over the MATERHORN rawinsonde launch site (EFS-Playa; Fig. 1) on 129 mostly clear days during the eight study months that were identified using the approach described below. Solar radiation is based on 1 October conditions. We examine the 2-m DTR from hourly output during a 24-h period beginning at 1800 UTC, which allows for a 4-h spinup.

3) RETROSPECTIVE SIMULATIONS

To examine the influence of soil moisture bias and the soil thermal conductivity parameterization used by Massey et al. (2014) on the morning and afternoon temperature biases in a fully cycled modeling system, we produce a series of retrospective 4DWX simulations for the MATERHORN fall field campaign period of 25 September–25 October 2012 (4DWX-MATERHORN). The MATERHORN fall field campaign period was relatively quiescent synoptically with limited precipitation (8.7 mm at the DPG National Weather Service Cooperative Observer site). The 4DWX-MATERHORN configuration is the same as the 2012 version of 4DWX-DPG except for use of 1) WRF v3.5.1, 2) updated data assimilation with the observation quality control done inside the model, 3) biweekly cold starts on Tuesdays and Fridays at 0500 UTC, and 4) climatological Great Salt Lake temperatures obtained from Steenburgh et al. (2000). Potentially important for the interpretation of these results is an upgrade of the YSU PBL parameterization between WRF v3.3.1 and WRF v3.5.1. Hu et al. (2013) note improved 2-m temperature forecasts with the YSU upgrade. We ran a 10-day comparison between the old and updated YSU schemes and also found 2-m temperature forecasts from the updated YSU scheme to outperform the old YSU scheme by only 15%. Therefore, we expect this to contribute only marginally to 2-m temperature error improvements between our retrospective simulations and 4DWX-DPG.

b. *Validation data and methods*

Near-surface 2-m temperature forecasts, which are diagnosed from the WRF surface driver, are validated against 2-m temperature observations obtained from the Mesowest cooperative networks (Horel et al. 2002). Although no formal quality control was performed on any of the 2-m observations, missing and obviously erroneous observations were removed. In addition, we only consider stations with a site elevation within 100 m of the corresponding WRF elevation, and observations reported within 5 min of the top of each hour. Stations are located primarily in valleys and basins. We use bias error (BE) to validate 4DWX forecasts against observations (BEO) or 4DWX analyses (i.e., forecast hour 0; BEA). BE is calculated as

$$\mathrm{BE} = \frac{1}{N}\sum_{i=1}^{N}(f_i - o_i),$$

where N is the number of forecast/observation pairs in the sample, f_i is the forecast, and o_i is the observation or analysis. Positive temperature BEs represent a warm bias, and negative temperature BEs represent a cold bias.

c. *Soil moisture observations*

Soil moisture observations used to validate 4DWX-DPG are taken from the North American Soil Moisture Database (NASMD) at Texas A&M University (http://soilmoisture.tamu.edu), which harmonizes and quality controls several in situ soil moisture observing platforms. Within the region encompassed by the 4DWX-DPG 10-km domain, the NASMD observations come from 27 U.S. Department of Agriculture Soil Climate Analysis Network (SCAN; Schaefer et al. 2007) stations and 15 global positioning system (GPS) soil moisture stations (Larson et al. 2008). SCAN stations use Stevens Water HydraProbes to measure soil moisture, and the probes are calibrated for each soil-texture class (Seyfried et al. 2005). Soil moisture is measured hourly at depths of 5.1, 10.2, 20.3, 50.8, and 101.6 cm, but the Noah LSM is configured with depths centered at 5, 25, 70, and 150 cm. Therefore, we only consider the 5.1- and 20.3-cm SCAN levels relative to the 5- and 25-cm Noah LSM levels, respectively, for initialization and validation. GPS stations receive L-band radiation (1.577 42 and 1.227 60 GHz) from GPS satellites, and the multipath signal that reflects off the land surface is used to calculate near-surface soil moisture (Ochsner et al. 2013). Unlike in situ measurements, such as those from SCAN, GPS soil moisture measurements represent a ~300 m^2 area, with some variation depending on the height of the GPS antenna (Larson et al. 2008). The GPS soil moisture measurements are influenced most strongly by 0–5-cm soil moisture in moist soils, but are more influenced by deeper soil moisture in drier soils. Rodriguez-Alvarez et al. (2009) found root-mean-square errors $< 0.03\ m^3 m^{-3}$ relative to 5-cm in situ observations, so we

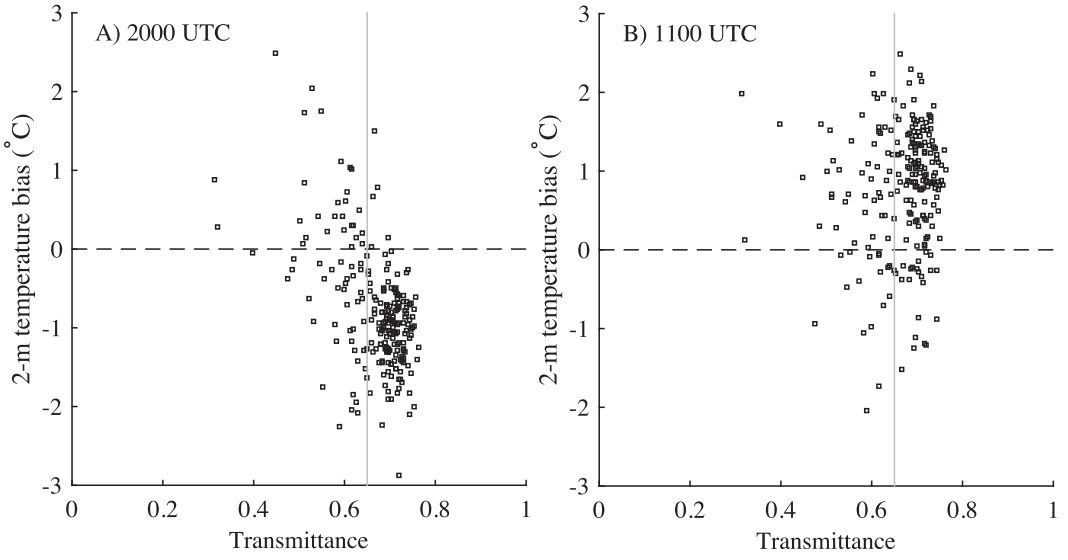

FIG. 3. Daily domain-averaged 4DWX-DPG 2-m temperature BEAs (°C) vs daily domain-averaged atmospheric transmittance for (a) 6-h forecasts ending at 2000 UTC and (b) 12-h forecasts ending at 1100 UTC.

conclude this dataset is useful for comparisons with 5-cm 4DWX-DPG soil moisture. Unfortunately, the NASMD data are not available from September and October 2014, limiting our 4DWX-DPG soil moisture validation to September and October during 2011–13.

3. Results

a. Bias error characteristics

The 2-m temperature BEOs from eight months of September and October operational 4DWX-DPG forecasts are −1.37°C in the afternoon [2000 UTC (1300 LST)] using 6-h forecasts (Fig. 2a) and 1.66°C in the early morning [1100 UTC (0400 LST)] using 12-h forecasts from 195 Mesowest stations in the 3.3-km domain (Fig. 2b).[1] An afternoon cold bias and early morning warm bias implies an underprediction of the amplitude of the 4DWX-DPG 2-m DTR. Although the early morning warm bias is slightly larger in magnitude than the afternoon cold bias, the early morning BEOs are especially large (>2°C) over valleys and basins, including the eastern sites of DPG, the Rush Valley, and the Wasatch Front (see Fig. 1 for locations). During the afternoon, nearly all sites have neutral or negative BEOs.

Daily 3.3-km domain-averaged afternoon 2-m temperature BEAs calculated from 6-h forecasts show a strong relationship between BEA and the domain-averaged atmospheric transmittance in the afternoon (Fig. 3a). Although the overall BEA for these forecasts is −0.77°C, on the 161 mostly clear days (i.e., transmittance > 0.65) the BEA is −1.01°C, whereas on the 67 mostly cloudy days the BEA is only −0.19°C. Only 5 mostly clear days have a warm bias, whereas 28 mostly cloudy days have a warm bias. An analysis of afternoon BEA sensitivity to wind speed, wind direction, and atmospheric stability yielded little to no correlation (not shown). These results suggest that the underestimation of the afternoon 2-m temperature might be related to the magnitude of the sensible, ground, and latent heat fluxes during the day. Although the signal is weaker, the early morning BEAs are also affected by sky cover. The overall BEA is 0.77°C, the mostly clear day BEA is 0.85°C, and the mostly cloudy day BEA is 0.57°C (Fig. 3b). This weaker influence may partly reflect the presence of nocturnal clouds prior to some mostly clear days.

Relative to 4DWX-DPG analyses, the afternoon 2-m temperature BEAs calculated from 6-h forecasts are negative throughout the domain on mostly clear days and strongest over eastern DPG and valleys to the southeast (Fig. 4a). During mostly cloudy days, the afternoon BEAs are weaker and even positive in some low-elevation basins and valleys (Fig. 4b). In contrast, the early morning 2-m temperature BEAs calculated from 12-h forecasts are primarily positive on mostly clear days except to the immediate west of the northern Great Salt Lake (Fig. 4c). These morning BEAs also exhibit more spatial variability than are found in the afternoon and are generally largest in valleys and basins.

[1] The 6- and 12-h forecasts are chosen for the afternoon and early morning, respectively, because they produce the largest BEs, as discussed later in this section. Times 2000 and 1100 UTC are chosen because they have the largest 2-m temperature biases.

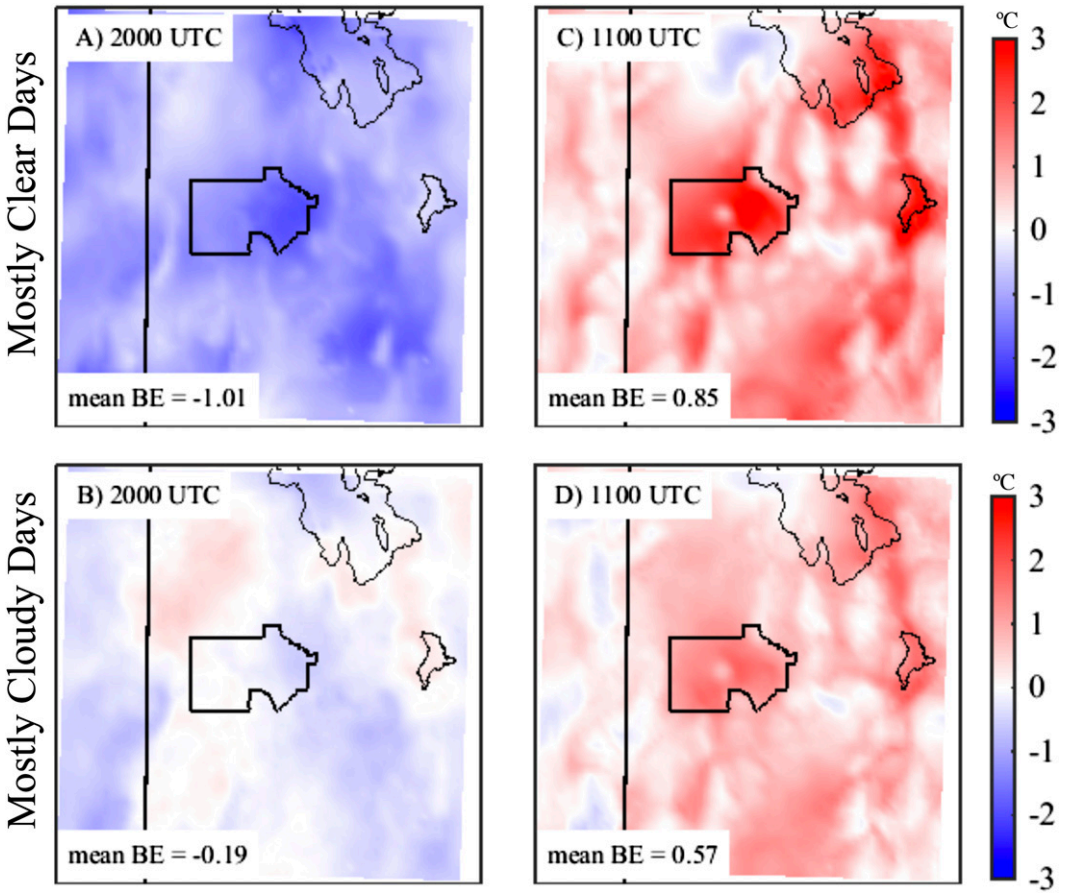

FIG. 4. Mean 4DWX-DPG 2-m temperature BEAs (°C) for (a) 2000 UTC on mostly clear days, (b) 2000 UTC on mostly cloudy days, (c) 1100 UTC on mostly clear days, and (d) 1100 UTC on mostly cloudy days. Overall mean BEA is annotated.

On mostly cloudy days, the early morning BEAs are weaker and more uniform (Fig. 4d). The spatial distribution and magnitude of the BEAs on mostly clear days are also similar to the BEOs (cf. Figs. 2 and 4), which justifies using 4DWX-DPG analyses for validation.

Comparison of mean observed and forecast (5–7 h) atmospheric soundings from EFS-Playa for the 15 soundings taken between 1800 and 0000 UTC during the MATERHORN fall 2012 field campaign show that the afternoon cold bias extends through 650 hPa (Fig. 5). The BEO reaches −1.53°C at 805 hPa. There is very little dewpoint temperature bias in the low levels, but a slight dry bias exists above 780 hPa. Forecast wind speeds are also close to the observations, but below 800 hPa the forecast winds are near northerly, whereas the observed are northeasterly or east-northeasterly.

EFS-Playa is located, however, over the playa of the western DPG (see Fig. 2 for location), which typically features higher soil moisture, higher thermal conductivity, and lower afternoon temperatures than over the surrounding sparsely vegetated desert, including the eastern DPG (Rife et al. 2002). We find weaker 2-m temperature BEOs over the playa than the surrounding region because of these differences (Fig. 2). Cross sections of potential temperature θ BEA calculated from 6-h forecasts show that the afternoon cold bias extends through the PBL and is maximized over eastern DPG (Fig. 6a; see Fig. 1 for cross-section location). In contrast, the early morning warm bias calculated from 12-h forecasts is confined primarily to the lowest model levels over the valleys and basins and is strongest below ~1500 m MSL (Fig. 6b). The 3.3-km domain-averaged potential temperature $\overline{\theta}$ BEA calculated between the lowest and 28th half-η levels (~surface–290 hPa) is −0.43 K in the afternoon and 0.21 K in the early morning. Thus, the afternoon cold bias has a greater impact on the regional tropospheric heat content than the early morning warm bias.

Mostly clear-day $\overline{\theta}$ BEAs not only show the diurnal modulation of BEAs, but also show an amplifying cold

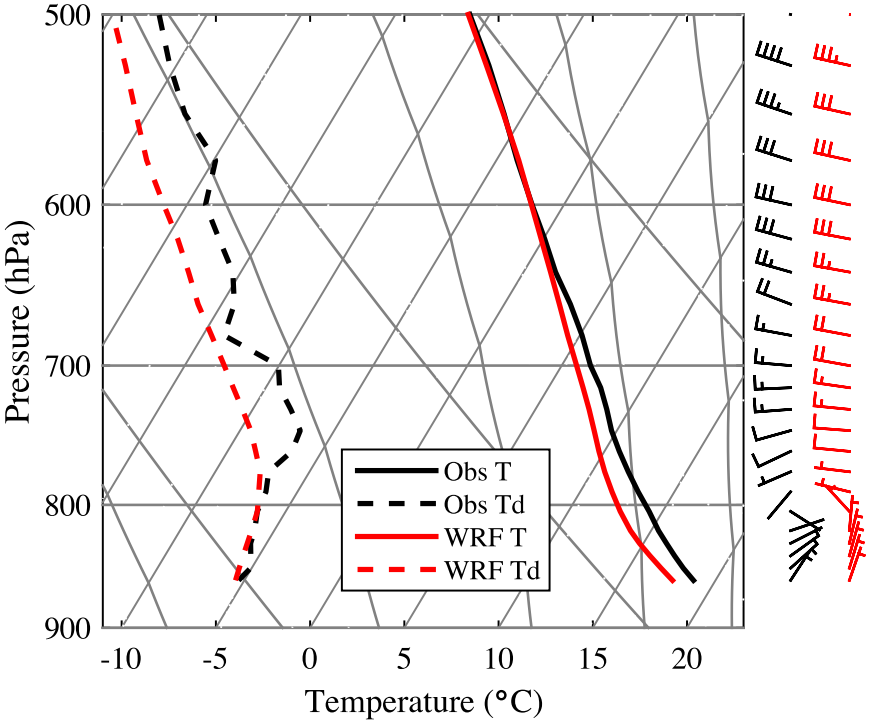

FIG. 5. Skew T–log$p$ diagrams of the mean of 15 soundings taken between 1800 and 0000 UTC during the MATERHORN fall field campaign from EFS-Playa (black) compared to the corresponding mean 4DWX-DPG values (red) using 5–7-h forecasts. Wind barbs ($m\,s^{-1}$) are shown where a half barb denotes 2.5 $m\,s^{-1}$ and full barb denotes 5 $m\,s^{-1}$.

bias with increasing forecast lead time regardless of initialization time (Fig. 7). For example, forecasts initialized at 0200 UTC have a $\overline{\theta}$ BEA maximum of 0.25 K at 1400 UTC on day 1 (12-h forecast) and a second maximum of −0.06 K at 1400 UTC on day 2 (36-h forecast). Similarly, forecasts initialized at other times have $\overline{\theta}$ BEA maxima at 1400 UTC on day 1 and day 2, as well as an intermediate minima at 2300 UTC. The use of 6- and 12-h forecasts to illustrate the afternoon and early morning BEAs throughout this chapter reflects the fact that the 2000 UTC cold bias is most pronounced in the 1400 UTC initialized run, and the 1100 UTC warm bias is most pronounced in the 2300 UTC initialized run, respectively.

b. *Near-surface soil moisture biases*

Mean 0000 UTC 5-cm soil moisture values during September and October of 2011–13 show that the

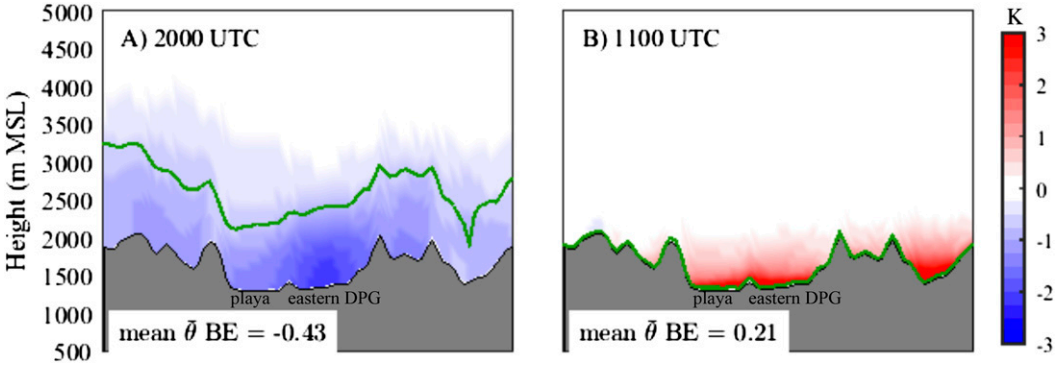

FIG. 6. Vertical cross sections of mean mostly clear-day 4DWX-DPG θ BEAs along dashed line in Fig. 1 at (a) 2000 and (b) 1100 UTC. The mean diagnosed PBL height (green line) and overall domain-wide $\overline{\theta}$ BEA are annotated.

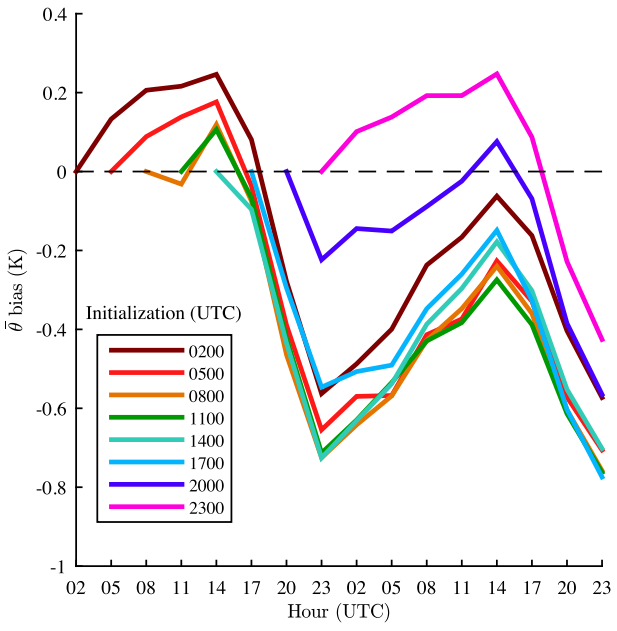

FIG. 7. Mostly clear-day $\bar{\theta}$ BEAs relative to 4DWX-DPG analyses for each nominal initialization time.

4DWX-DPG analyses have a pronounced regional-scale moist bias compared to the 42 NASMD stations throughout the intermediate 10-km domain (Fig. 8), with similar biases in the 30- and 3.3-km domains (not shown). The NASMD station located within DPG has the highest mean soil moisture, yet is still drier than the 4DWX-DPG analyses. The NASMD stations also exhibit more spatial variability than does the 4DWX-DPG-analyzed soil moisture, with a range of 0.007–0.198 $m^3 m^{-3}$ compared to 0.172–0.256 $m^3 m^{-3}$, respectively. The GPS stations have a smaller range (0.049–0.133 $m^3 m^{-3}$) than the SCAN stations (0.007–0.198 $m^3 m^{-3}$), but a similar mean (0.093 $m^3 m^{-3}$ compared to 0.099 $m^3 m^{-3}$). Although the focus of this study is on the net contribution of soil moisture to temperature bias, we anticipate soil moisture analyses that capture this spatial variability will further improve temperature forecasts.

The mean 4DWX-DPG 5-cm soil moisture at all NASMD station locations during September and October of 2011–13 is 0.223 $m^3 m^{-3}$, compared to an observed mean of only 0.096 $m^3 m^{-3}$. Bias correcting by reducing the 4DWX-DPG 5-cm soil moisture by this 0.127 $m^3 m^{-3}$ difference yields a close match for daily values (Fig. 9), although a slight moist bias remains during and immediately following some precipitation events.[2] A similar analysis was conducted for the 25-cm soil moisture, yielding a 0.079 $m^3 m^{-3}$ moist bias (not shown). The mean 4DWX-DPG 25-cm soil moisture is 0.215 $m^3 m^{-3}$, and the mean 20.3-cm SCAN soil moisture is 0.137 $m^3 m^{-3}$. Since the 4DWX-DPG soil moisture analyses are set to GFS analysis values during weekly cold starts and change very little during the week, these soil moisture biases originate with the GFS analyses.

[2] Precipitation events are inferred from rapid soil moisture increases.

c. SCM simulations

We use the SCM to test the sensitivity of the 2-m DTR, which is underpredicted in 4DWX-DPG, to the 5-cm soil moisture, the specification of C_{zil}, the choice of long- and shortwave radiation schemes, and the choice of PBL scheme. Changes in DTR are influenced by both nighttime and daytime temperature changes. We test over the three most common land-use and soil-texture class combinations in the 3.3-km domain: shrubland with loam soil (S-L), shrubland with silt loam soil (S-SL), and playa with playa soil (P-P). S-SL is also tested using the standard Noah LSM and a modified version (S-SL-m) that incorporates the McCumber and Pielke (1981) soil thermal conductivity parameterization (MP81) for silt loam and sandy loam soils, which was shown by Massey et al. (2014) to improve the early morning warm bias over DPG.

1) SOIL MOISTURE

In our SCM simulations over the range of allowable near-surface soil moistures in the Noah LSM (0.02–0.48 $m^3 m^{-3}$), the 2-m DTR increases rapidly with decreasing soil moisture, especially at lower soil moistures (e.g., <0.15 $m^3 m^{-3}$; Fig. 10a). A soil moisture decrease from 0.22 $m^3 m^{-3}$ (the approximate mean 4DWX-DPG soil moisture) to 0.10 $m^3 m^{-3}$ (the approximate mean NASMD soil moisture) yields 2-m DTR increases of 2.5°C for S-L, 3.1°C for P-P, 2.5°C for S-SL, and 5.4°C for S-SL-m. The mean 2-m DTR for S-L, P-P, and S-SL-m is 16.4°C at 0.10 $m^3 m^{-3}$, which is 2.5°C higher than the maximum obtained in any other SCM experiment (Figs. 10b–d). These results strongly suggest that the soil moisture bias and the default parameterization of soil thermal conductivity are significant contributors to the 2-m DTR underprediction.

2) ZILITINKEVICH COEFFICIENT C_{ZIL}

Another potential contributor to the 2-m DTR errors in 4DWX-DPG is the uncertainty associated with estimating C_{zil}. The relationship between the roughness lengths for heat z_{0t} and momentum z_{0m} in the Noah LSM currently follows Zilitinkevich (1995):

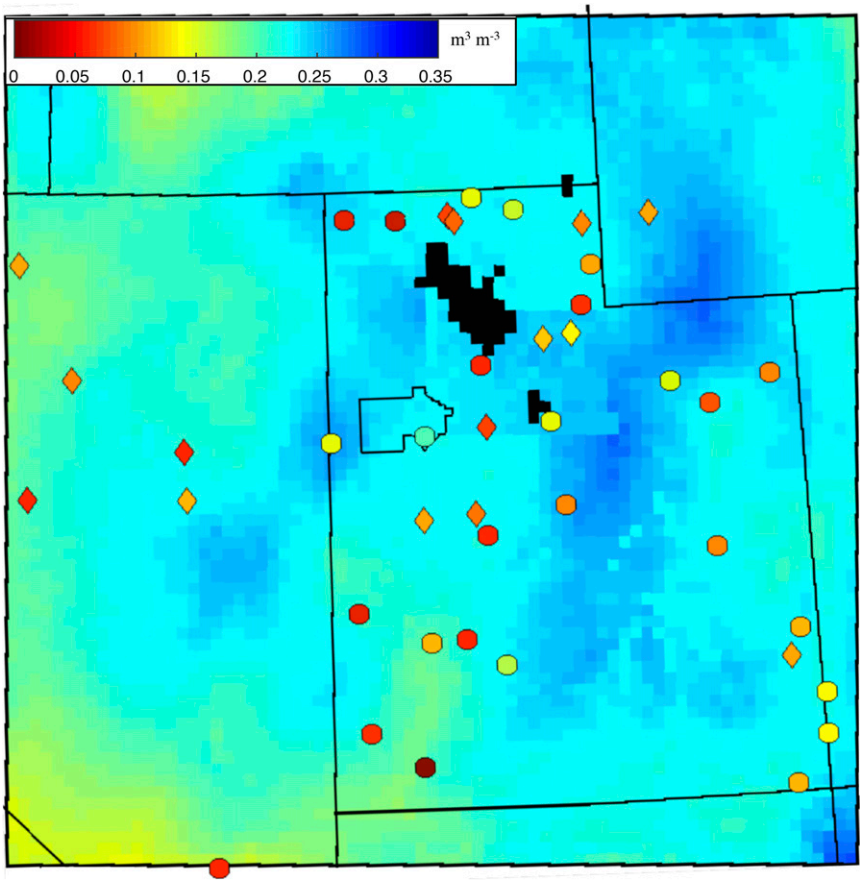

FIG. 8. Mean 0000 UTC 5-cm soil moisture (or equivalent) from the 4DWX-DPG 10-km domain and NASMD stations (SCAN, circles; GPS, diamonds) during September and October 2011–13.

$$z_{0t} = z_{0m} \exp(-kC_{\text{zil}}\sqrt{R_e}),$$

wherein $k = 0.4$ is the von Kármán constant and R_e is the roughness Reynolds number. In addition, C_{zil} serves as an empirical coefficient that helps control the surface heat exchange with the atmosphere. During the day, higher C_{zil} values lead to higher surface skin temperatures, lower surface sensible heat fluxes, and lower atmospheric temperatures (Zheng et al. 2012; Zeng et al. 2012).

Previous WRF versions of the Noah LSM employed a constant C_{zil} of 0.1, but Chen and Zhang (2009) implemented an option for using the following relationship, which was incorporated into 4DWX-DPG:

$$C_{\text{zil}} = 10^{[-0.4(z_0/0.07)]},$$

wherein z_0 is the roughness length of the underlying land-use category. A realistic range of C_{zil} is between 0, which assumes an identical z_{0t} and z_{0m}, and 1 (Chen et al. 1997).

In our SCM simulations, the 2-m DTR increases with decreasing C_{zil} at a nearly constant rate for all four simulations (Fig. 10b). The mean maximizes at 13.9°C when C_{zil} is zero (Fig. 10b). This is 2.5°C lower than the mean 2-m DTR at a 0.10 $\text{m}^3\,\text{m}^{-3}$ soil moisture (cf. Figs. 10a,b). In addition, the low roughness lengths of S-L, S-SL, and P-P over DPG imply a higher C_{zil} value (Chen and Zhang 2009), so a C_{zil} of zero is unlikely. Therefore, errors stemming from the estimation of C_{zil} are not contributing significantly to the underestimation of the 2-m DTR in 4DWX-DPG.

3) RADIATION SCHEMES

Long- and shortwave radiation schemes have a minor influence on the 2-m DTR, and only the Community Atmosphere Model schemes (CAM; Collins et al. 2004) increase the mean 2-m DTR (by 1.5°C or less) compared

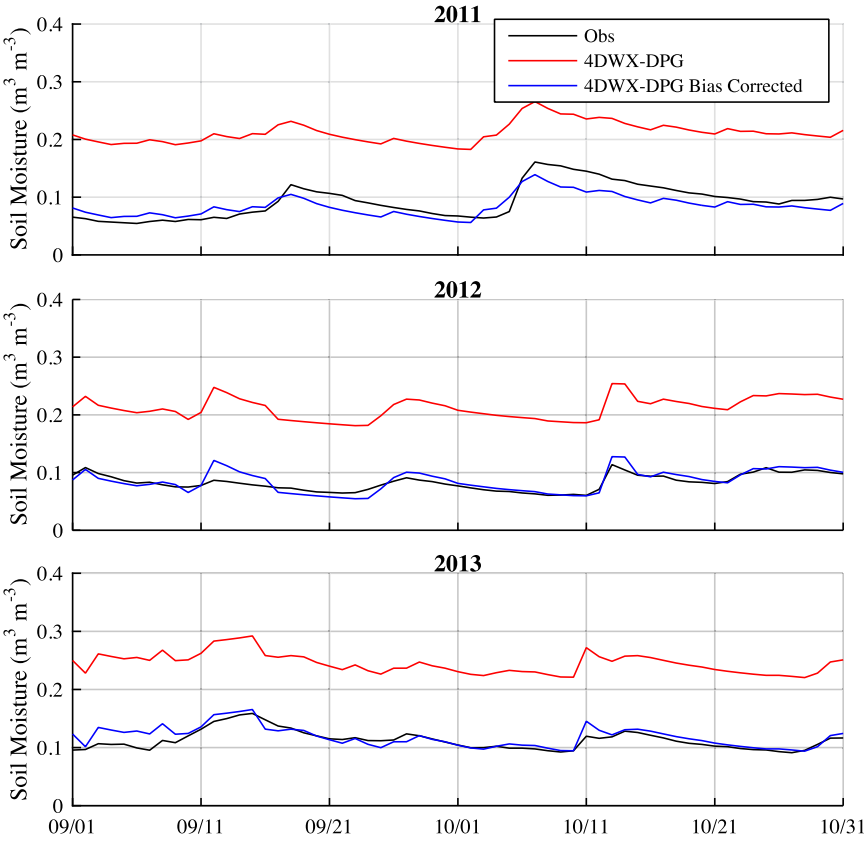

FIG. 9. Mean daily observed (black), 4DWX-DPG (red), and 4DWX-DPG bias-corrected (blue) 5-cm soil moisture for all NASMD stations in the 10-km domain.

to the RRTM and Dudhia schemes currently used in 4DWX-DPG (Fig. 10c; S-SL not presented). The 2-m DTR decreases marginally compared to RRTM and Dudhia using the global climate model version of the RRTM schemes (RRTMG; Iacono et al. 2008) or the Goddard schemes (Chou and Suarez 1999). We conclude that none of the radiation schemes tested significantly increases the DTR compared to the RRTM and Dudhia schemes currently used in 4DWX-DPG.

4) PBL SCHEMES

Here, we test first-order, nonlocal, and 1.5-order TKE closure schemes that were also tested by Zhang et al. (2013) over the DPG region. The quasi-normal scale elimination PBL scheme (QNSE; Sukoriansky et al. 2005) and the Mellor–Yamada–Nakanishi–Niino level-2.5 PBL scheme (MYNN2; Nakanishi and Niino 2004) are 1.5-order TKE schemes and produce slightly higher mean 2-m DTRs than the YSU scheme currently used in 4DWX-DPG (Fig. 10d). The Asymmetric Convective Model version 2 scheme (ACM2; Pleim 2007) and the Mellor–Yamada–Janjić (MYJ) turbulent kinetic energy (TKE) scheme (Mellor and Yamada 1982) produce slightly lower DTRs than the YSU scheme. The small changes suggest that none of the PBL schemes presently available in WRF will significantly increase the DTR compared to the YSU scheme currently used in 4DWX-DPG. These results are consistent with the findings of Zhang et al. (2013).

d. Retrospective simulations

Motivated by the results above, we test the influence of the overestimation of near-surface soil moisture on temperature forecasts in the fully cycled retrospective 4DWX-MATERHORN simulations. Table 1 summarizes the three different retrospective cycles, which use varying soil thermal conductivity parameterizations and varying regions of bias-corrected near-surface soil moisture. The control 4DWX-MATERHORN cycle that is initialized from GFS soil moisture analyses and uses the default WRF soil thermal conductivity parameterization (hereafter referred to as Control) has afternoon and early morning 2-m temperature BEOs

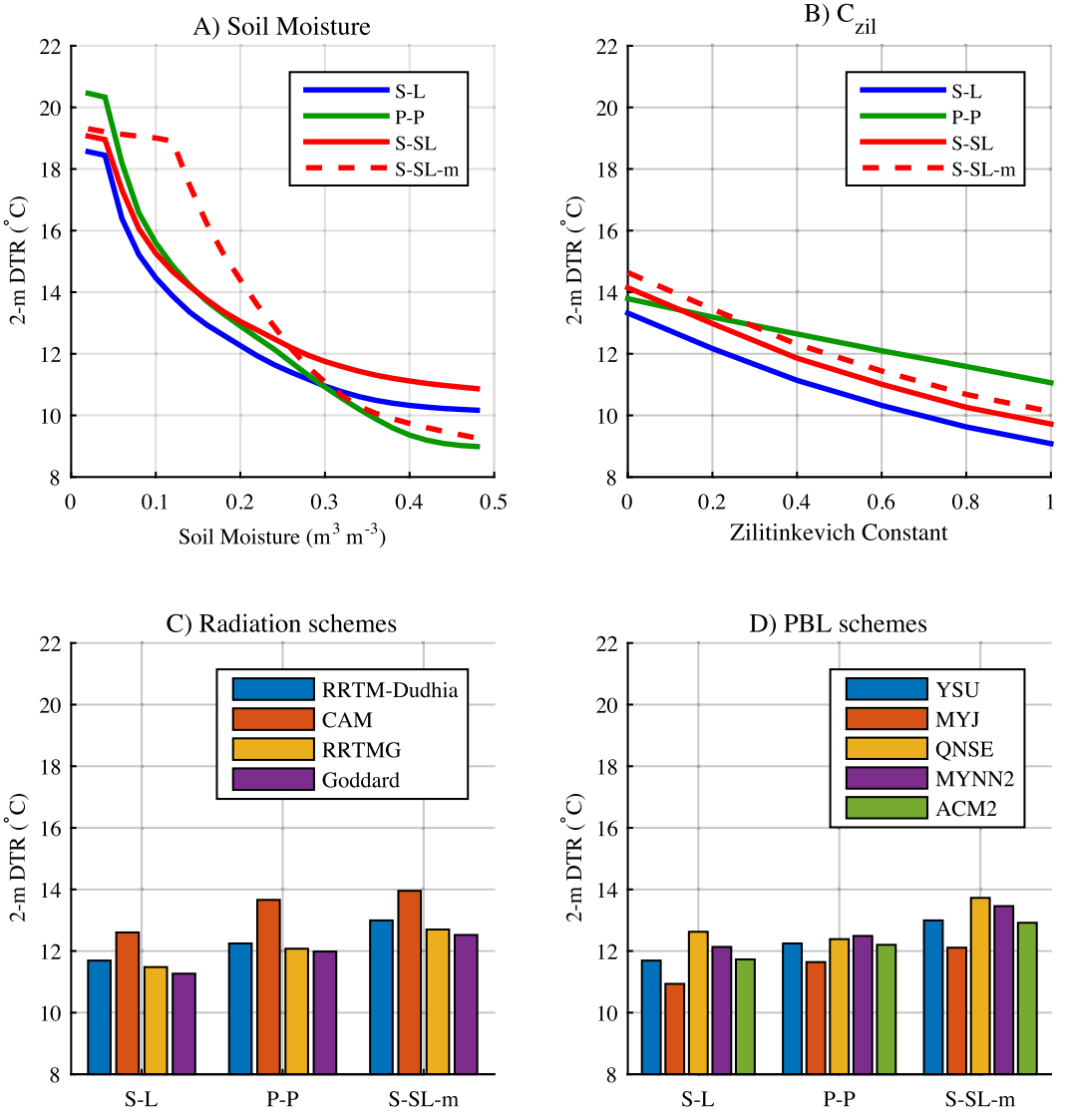

FIG. 10. The 2-m temperature DTR calculated from hourly SCM output for the 23-h period between 1800 and 1700 UTC as a function of (a) soil moisture, (b) Zilitinkevich constant, (c) long- and shortwave radiation schemes, and (d) PBL scheme. Simulations are initialized with S-L, S-SL, and P-P land surfaces.

of −1.62°C (Fig. 11a) and 1.93°C (Fig. 11b), respectively, which are similar to, but slightly larger than, the BEOs produced by 4DWX-DPG for all eight validation months (cf. Figs. 2 and 11). Spatially, the BEO distributions are also similar.

In the SM-d03 simulations, we bias correct by reducing the 5-cm soil moisture analyses of the 3.3-km domain by 0.131 $m^3 m^{-3}$ and by reducing the 25-cm analyses by 0.072 $m^{-3} m^{-3}$. The soil moisture reduction was calculated by subtracting the 4DWX-DPG values corresponding to NASMD stations from the observations within the region encompassed by the 10-km domain during the MATERHORN period. Following Massey et al. (2014), we also replace the soil thermal conductivity parameterization in the Noah LSM with MP81 for silt loam and sandy loam soils. These changes reduce the afternoon and morning 2-m temperature BEOs to −0.90°C (Fig. 11c) and 0.64°C (Fig. 11d), improvements of 0.72° and 1.29°C relative to Control, respectively. In both cases, the greatest improvement occurs over DPG, with less improvement along the Wasatch Front. The Wasatch Front is urbanized and irrigated, and the bias-corrected soil moisture might not be representative over this area. Overall, SM-d03 improves the early morning warm bias, but the afternoon cold bias improvement is smaller.

TABLE 1. Summary of 4DWX-MATERHORN simulations.

	Control	SM-d03	SM-Full
Soil moisture initialization at cold start	1.0° GFS analysis	Bias corrected on 3.3-km domain	Bias corrected on 3.3-, 10-, and 10-km footprints in 30-km domains
Noah LSM modifications	None	MP81 for silt loam and sandy loam soils	MP81 for silt loam and sandy loam soils

The SM-Full simulations are similar to those for SM-d03 except the soil moisture bias corrections are applied to the 3.3-km domain, the 10-km domain, and the 10-km domain's footprint in the 30-km domain. This results in drier and more realistic soil moistures across the broader Intermountain West. These changes reduce the afternoon and morning BEOs to −0.34°C (Fig. 11e) and 0.57°C (Fig. 11f), improvements of 0.56°C, and 0.07°C relative to SM-d03, respectively. Thus, the afternoon cold bias improves from both local and regional soil moisture bias correction, but the early morning warm bias is more sensitive to local soil moisture, with little improvement from soil moisture bias correction over the broader region. This result is consistent with the greater depth and regional coverage of the afternoon cold bias.

Hourly 2-m temperature BEOs calculated from 11–14-h forecasts illustrate the underestimation of the 2-m DTR in Control, greatly improved nighttime forecasts in SM-d03, and greatly improved nighttime and daytime forecasts in SM-Full (Fig. 12). The mean 1700–0000 UTC daytime cold bias is −1.17°C in Control and improves to −0.68°C in SM-d03 and −0.20°C in SM-Full. The 0300–1400 UTC mean nighttime warm bias is 1.26°C in Control and improves to 0.23° and 0.33°C in SM-d03 and SM-Full, respectively. However, SM-d03 and SM-Full introduce a brief morning-transition [1500 UTC (0800 LST)] warm bias and evening-transition [0100 UTC (1800 LST)] cold bias. These BEOs may be related to the inaccurate partitioning of the surface energy budget in conjunction with PBL evolution during the transitions, which should be investigated in future work.

The 2-m temperature BEAs have a local maximum near 1400 UTC and local minimum at 2000 UTC in Control for forecasts initialized at all nominal 4DWX-MATERHORN initialization times, but local maxima and minima are nearly eliminated in SM-Full (Fig. 13). Therefore, the diurnal modulation of 2-m BEAs is almost nonexistent in SM-Full. However, an overall amplifying cold bias with increasing forecast lead time exists in both Control and SM-Full, similar to the amplifying cold bias observed in 4DWX-DPG (cf. Figs. 7 and 13), suggesting the presence of an unknown diurnally independent error source.

Comparison of mean MATERHORN atmospheric soundings taken between 1800 and 0000 UTC at EFS-Playa with corresponding 5–7-h Control forecast soundings shows a deep cold bias (Fig. 14, red line) that was also present in the original 4DWX-DPG forecasts. The SM-Full forecasts (blue line) more closely match observations above 800 hPa, but exhibit a warm bias near the surface. This warm bias is consistent with positive 2000 UTC 2-m temperature biases at playa stations in SM-Full (Fig. 11e). The use of a spatially homogeneous soil moisture bias correction based on data collected from the surrounding region may not be appropriate over this unique land surface type.

Cross sections of θ BEAs calculated from 6- and 12-h forecasts during the afternoon and early morning, respectively, also show temperature improvements in SM-d03 and SM-Full compared to Control (Fig. 15). Control has similar BEAs to 4DWX-DPG with an afternoon cold bias extending through the depth of the mean PBL and into the middle troposphere, yielding a $\overline{\theta}$ of −0.54°C. In contrast, the early morning warm bias is confined to the lowest few model levels in valleys and basins (cf. Figs. 6 and 15a,b), yielding a $\overline{\theta}$ of 0.12°C. Compared to 4DWX-DPG forecasts for the entire 8-month validation period, $\overline{\theta}$ features a stronger afternoon cold bias and a weaker early morning warm bias, consistent with the stronger overall amplifying cold bias that exists in the 4DWX-MATERHORN simulations compared to the 4DWX-DPG forecasts for the entire 8-month validation period (cf. Figs. 15a,b and Figs. 6a,b). The SM-d03 experiment reduces the overall afternoon cold bias (Fig. 15c) and nearly eliminates the strong early morning warm BEAs in the lowest few model levels (Fig. 15d). The SM-Full simulation further reduces the mean afternoon $\overline{\theta}$ cold bias (Fig. 15e) and largely eliminates the early morning near-surface warm bias (Fig. 15f). In SM-d03 and SM-Full, an upper-level cold bias develops with increasing forecast lead time as the near-surface BEAs improve. We hypothesize that the upper-level cold bias, which is also observed at 2 m (Fig. 13), is related to erroneous lateral boundary conditions from the outer domains given the vertical extent of the error.

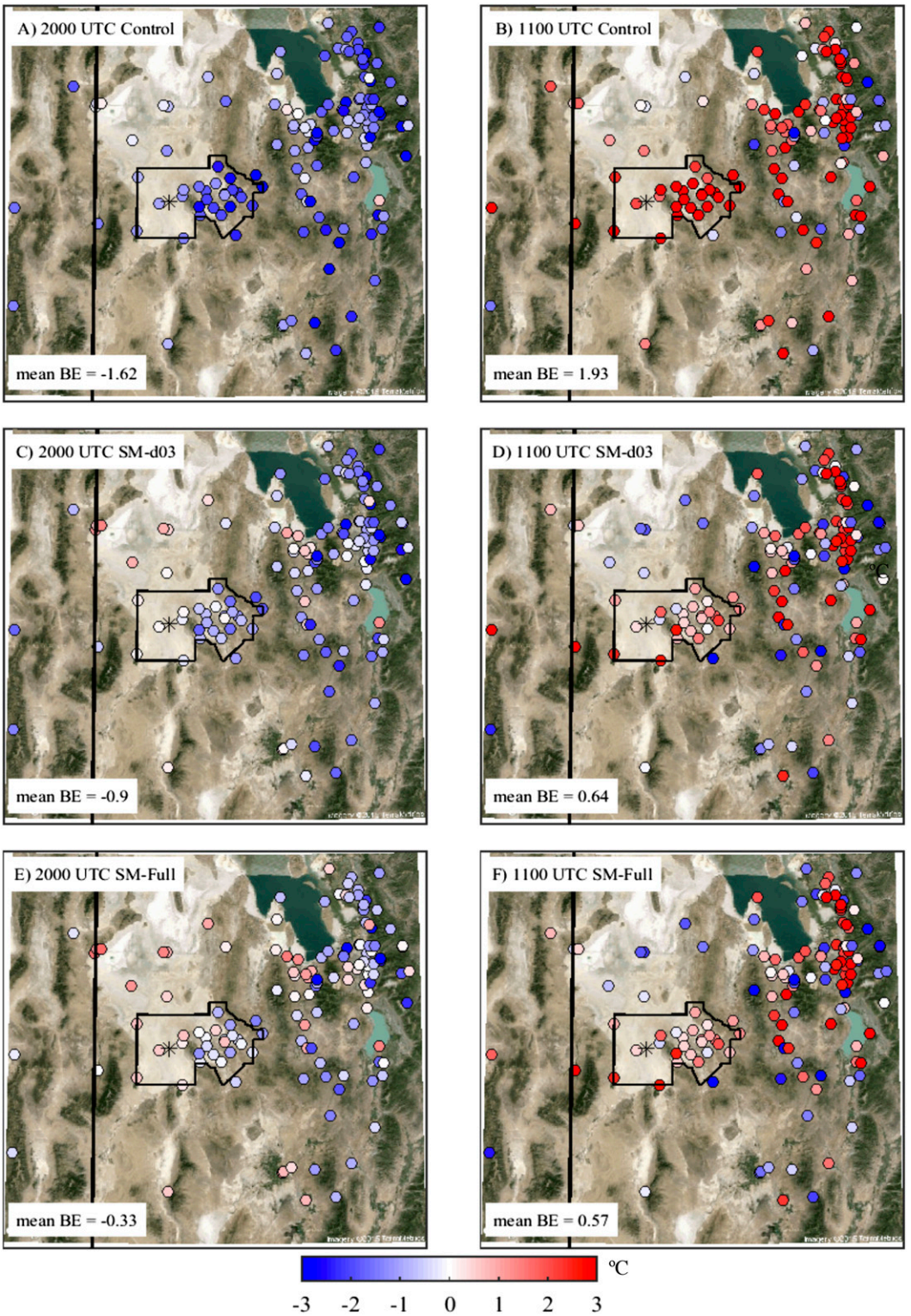

FIG. 11. As in Fig. 2, but for the (a),(b) Control, (c),(d) SM-d03, and (e),(f) SM-Full simulations of 4DWX-MATERHORN.

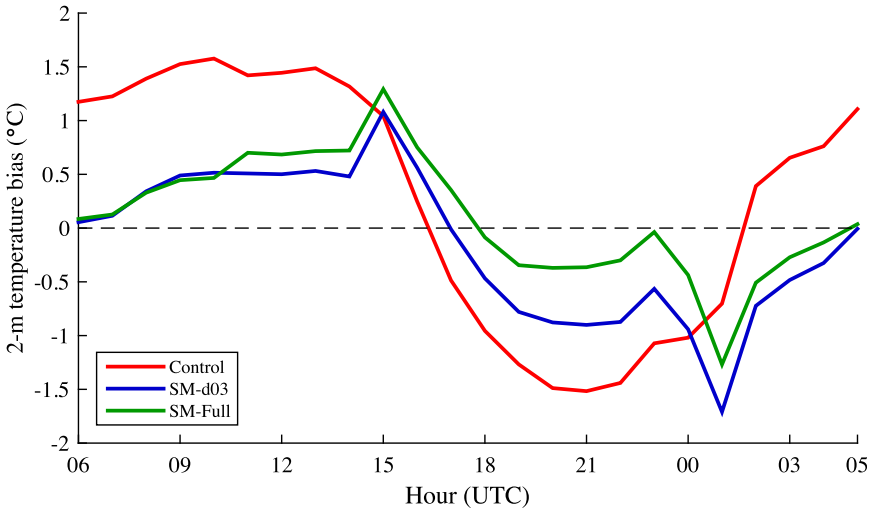

FIG. 12. Mean 11–14-h 2-m temperature BEOs from Control (red), SM-d03 (blue), and SM-Full (green) at MesoWest stations during the 4DWX-MATERHORN period.

Time–height cross sections of θ during the fifth intensive operating period of the MATERHORN fall 2012 field campaign (2100 UTC 9 October–1200 UTC 10 October 2012) are created from 3-hourly observed EFS-Playa soundings (Fig. 16a), the 1100 UTC 9 October 2012 Control simulation (Fig. 16b), and the 1100 UTC 9 October 2012 SM-Full simulation (Fig. 16c). This period has the most consecutive successful soundings during the MATERHORN fall 2012 field campaign. The θ differences between the observations and Control show a large underprediction of θ (Fig. 16b), whereas SM-Full shows θ within 1 K of observations (Fig. 16c). In addition to the improved θ forecasts, SM-Full also improves the 800–700-hPa atmospheric stability (cf. Figs. 16a and 16c), which is overpredicted in Control (cf. Figs. 16a and 16b). Therefore, SM-Full may improve forecasts of other meteorological phenomena dependent on atmospheric stability such as winds and cloud development.

4. Summary and conclusions

Eight months of operational WRF forecasts underpredict the strength of the diurnal temperature range (DTR) for Dugway Proving Ground in northwestern Utah (4DWX-DPG) during September and October of 2011–14. During the afternoon [2000 UTC (1300 LST)], the 2-m temperature bias error (BE) in 12-h forecasts is −1.37°C relative to observations, with the cold bias extending through the top of the mean planetary boundary layer. In the early morning [1100 UTC (0400 LST)], the 2-m temperature BE in 6-h forecasts is 1.66°C, but the warm bias is confined to the lowest few model levels in valleys and basins. The BEs are greatest during mostly clear skies.

The underprediction of the 2-m DTR is primarily the result of an overestimation of near-surface soil moisture in 4DWX-DPG analyses, which is initialized from the Global Forecast System (GFS) analyses once per week. The 4DWX-DPG system overestimates the 5- and 25-cm soil moisture by mean values of 0.127 and

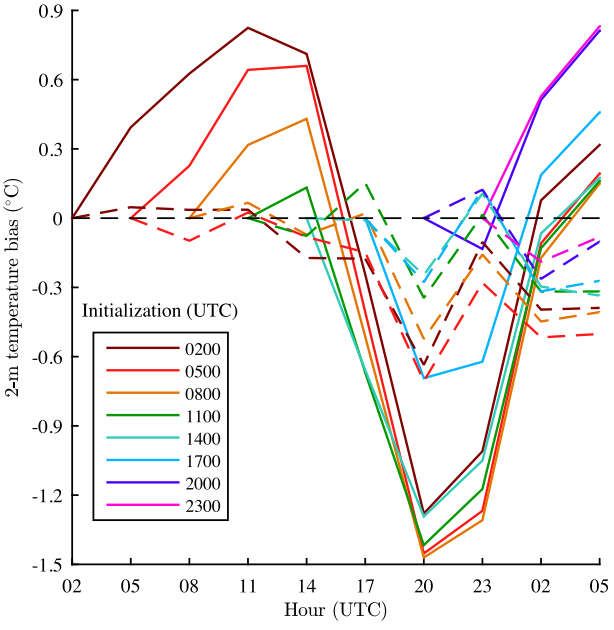

FIG. 13. Mean 2-m temperature BEAs for each nominal initialization time from Control (solid lines) and SM-Full (dashed lines) during the 4DWX-MATERHORN period.

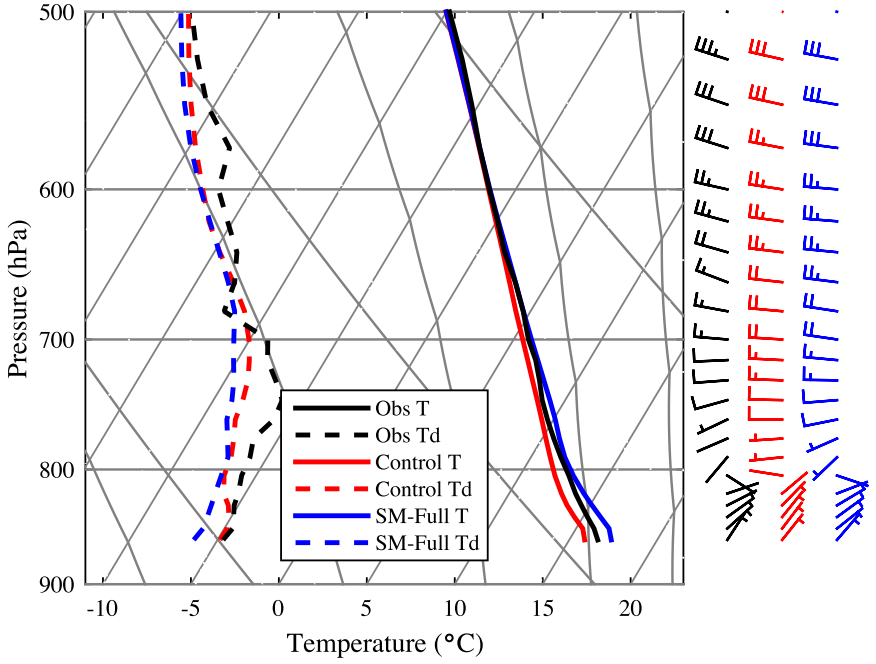

FIG. 14. As in Fig. 5, but for Control (red) and SM-Full (blue).

$0.079\,m^3\,m^{-3}$, respectively, compared to 42 North American Soil Moisture Database (NASMD) soil moisture observing stations. These biases are fairly consistent over a 6-month period enabling straightforward bias correction of 4DWX-DPG soil moisture analyses. Results from WRF single-column model (SCM) simulations illustrate that bias-corrected soil moisture combined with the McCumber and Pielke (1981) soil thermal conductivity parameterization for silt loam and sandy loam soils (Massey et al. 2014) greatly improves the 2-m DTR forecast. The planetary boundary layer schemes, radiation schemes, and the estimation of the Zilitinkevich coefficient have a smaller influence on 2-m DTR.

Retrospective simulations for the MATERHORN fall 2012 field campaign period (4DWX-MATERHORN) show improved temperature forecasts using bias-corrected soil moisture analyses and a modified soil thermal conductivity parameterization. When the bias correction is only applied to the innermost 3.3-km domain (SM-d03), the early morning warm bias is nearly eliminated, but the afternoon cold bias is only slightly reduced. When the bias correction is applied regionally to the 3.3-km domain, the 10-km domain, and the 10-km domain's footprint in the 30-km domain (SM-Full), the afternoon cold bias is nearly eliminated. These results imply that the early morning warm bias is most sensitive to the local soil moisture, whereas the afternoon cold bias is sensitive to both the local and regional soil moisture. SM-Full also produces improvements in atmospheric temperature and stability above the surface.

Although the use of bias-corrected soil moisture yields significant 2-m temperature forecast improvements, an amplifying tropospheric cold bias develops in all simulations. The causes of this cold bias are unknown, but may be related to erroneous lateral boundary conditions or the 4DWX configuration. Both SM-d03 and SM-Full also introduce a brief 2-m temperature warm bias during the morning transition [1500 UTC (0800 LST)] and cold bias during the evening transition [0100 UTC (1800 LST)]. The source of these errors should be investigated in future work.

These results highlight a major consequence of the use of global soil moisture analyses for regional temperature prediction. These analyses, and others such as those produced by the National Centers for Environmental Prediction (NCEP) GFS or the European Centre for Medium-Range Weather Forecasts (ECMWF) Integrated Forecast System (IFS), rely on land surface models that do not currently assimilate or utilize soil moisture observations. Over the Intermountain West, this leads to a large positive soil moisture bias that degrades temperature forecasts. Other regions may have similarly large soil moisture biases and associated temperature forecasts errors. The global soil moisture analyses can potentially be improved by incorporating existing in situ soil moisture observations. Deployment of more soil moisture stations should also be considered

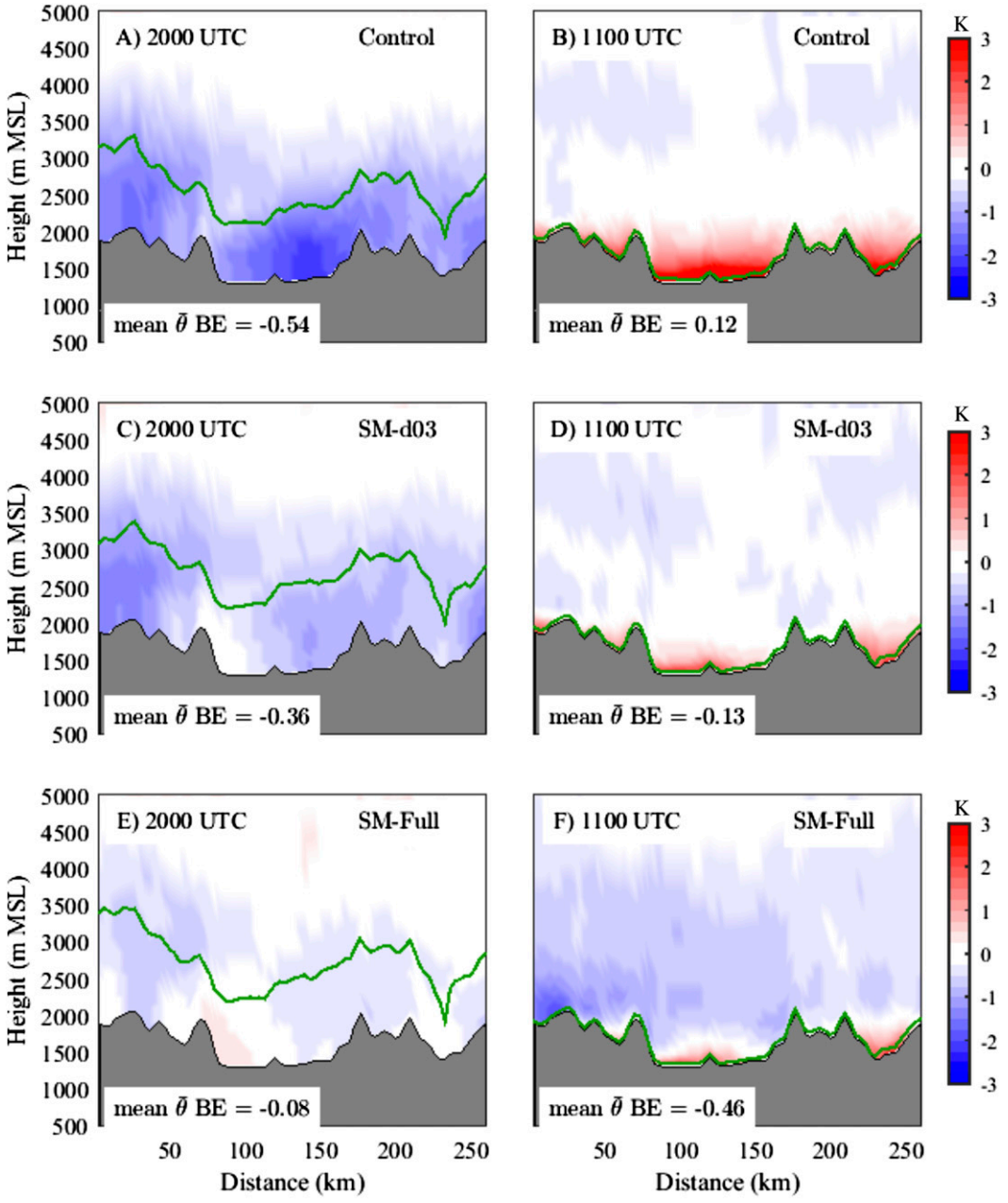

FIG. 15. As in Fig. 6, but for (a),(b) Control, (c),(d) SM-d03, and (e),(f) SM-Full.

over data-sparse regions, especially the cost-effective GPS-based stations. The recently launched NASA Soil Moisture Active/Passive (SMAP) mission, which provides remotely sensed soil moisture data in 9-km pixels, much finer than previous satellite-based soil moisture estimates, also offers significant potential to improve soil moisture analyses worldwide.

Acknowledgments. This research was funded by Office of Naval Research Award N00014-11-1-0709, the Mountain Terrain Atmospheric Modeling and Observations (MATERHORN) Program, and by the U.S. Army Test and Evaluation Command (ATEC) through an interagency agreement with the National Science Foundation. We thank our fellow MATERHORN participants, especially Sebastian Hoch for collecting and processing the rawinsonde data, and John Horel, Zhaoxia Pu, Joshua Hacker, Fotini Chow, Stephan de Wekker, and Dave Whiteman for their input and contributions. We also thank Trenton Ford and Steven

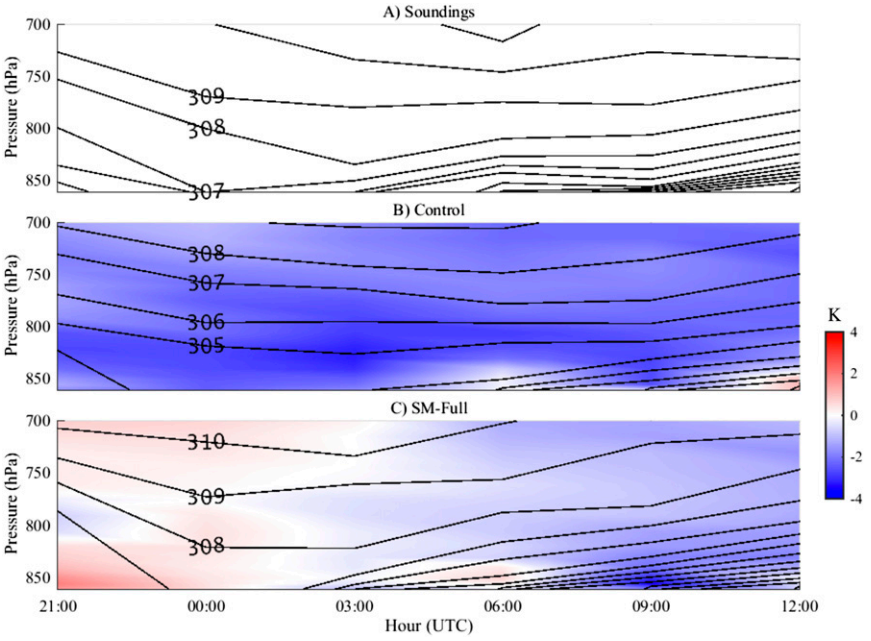

FIG. 16. Time–height sections of θ (contours every K) and bias (color fill based on scale at right) from 2100 UTC 9 Oct to 1200 UTC 10 Oct 2012. (a) Observed 3-h soundings from EFS-playa, (b) Control, and (c) SM-Full. Control and SM-Full are initialized at 1100 UTC 9 Oct 2012.

Quiring for providing the North American Soil Moisture Database data, Erik Crosman and Leah Campbell for their WRF expertise, and three anonymous reviewers for comments and suggestions that significantly improved the manuscript.

REFERENCES

Albergel, C., P. de Rosnay, G. Balsamo, L. Isaksen, and J. Muñoz-Sabater, 2012a: Soil moisture analyses at ECMWF: Evaluation using global ground-based in situ observations. *J. Hydrometeor.*, **13**, 1442–1460, doi:10.1175/JHM-D-11-0107.1.

——, ——, C. Gruhier, J. Muñoz-Sabater, S. Hasenauer, L. Isaksen, Y. Kerr, and W. Wagner, 2012b: Evaluation of remotely sensed and modelled soil moisture products using global ground-based in situ observations. *Remote Sens. Environ.*, **118**, 215–226, doi:10.1016/j.rse.2011.11.017.

Al Bitar, A., D. Leroux, Y. H. Kerr, O. Merlin, P. Richaume, A. Sahoo, and E. F. Wood, 2012: Evaluation of SMOS soil moisture products over continental U.S. using the SCAN/SNOTEL network. *IEEE Trans. Geosci. Remote Sens.*, **50**, 1572–1586, doi:10.1109/TGRS.2012.2186581.

Banta, R. M., and P. T. Gannon, 1995: Influence of soil moisture on simulations of katabatic flow. *Theor. Appl. Climatol.*, **52**, 85–94, doi:10.1007/BF00865509.

Chen, F., and J. Dudhia, 2001: Coupling an advanced land surface–hydrology model with the Penn State–NCAR MM5 modeling system. Part I: Model implementation and sensitivity. *Mon. Wea. Rev.*, **129**, 569–585, doi:10.1175/1520-0493(2001)129<0569:CAALSH>2.0.CO;2.

——, and Y. Zhang, 2009: On the coupling strength between the land surface and the atmosphere: From viewpoint of surface exchange coefficients. *Geophys. Res. Lett.*, **36**, L10404, doi:10.1029/2009GL037980.

——, Z. Janjić, and K. Mitchell, 1997: Impact of atmospheric surface-layer parameterization in the new land-surface scheme of the NCEP mesoscale Eta Model. *Bound.-Layer Meteor.*, **85**, 391–421, doi:10.1023/A:1000531001463.

Cheng, W. Y. Y., and W. J. Steenburgh, 2005: Evaluation of surface sensible weather forecasts by the WRF and the Eta Models over the western United States. *Wea. Forecasting*, **20**, 812–821, doi:10.1175/WAF885.1.

Chou, M.-D., and M. J. Suarez, 1999: A solar radiation parameterization for atmospheric studies. NASA Tech. Rep. Series on Global Modeling and Data Assimilation, NASA/TM-1999-104606, Vol. 15, 40 pp.

Collins, W. D., P. J. Rasch, B. A. Boville, J. J. Hack, J. R. McCaa, D. L. Williamson, J. T. Kiehl, and B. Briegleb, 2004: Description of the NCAR Community Atmosphere Model (CAM2). NCAR Tech. Note NCAR/TN–464+STR, 214 pp. [Available online at http://www.cesm.ucar.edu/models/atm-cam/docs/description/description.pdf.]

Crow, W. T., D. G. Miralles, and M. H. Cosh, 2010: A quasi-global evaluation system for satellite-based surface soil moisture retrievals. *IEEE Trans. Geosci. Remote Sens.*, **48**, 2516–2527, doi:10.1109/TGRS.2010.2040481.

Daniels, M. H., F. K. Chow, and G. S. Poulos, 2006: Effects of soil moisture initialization on simulations of atmospheric boundary layer evolution in Owens Valley. Preprints, *12th Conf. on Mountain Meteorology*, Santa Fe, NM, Amer. Meteor. Soc., 7.2. [Available online at http://ams.confex.com/ams/pdfpapers/114757.pdf.]

Dee, D. P., M. Balmaseda, G. Balsamo, R. Engelen, A. J. Simmons, and J.-N. Thépaut, 2014: Toward a consistent reanalysis of the climate system. *Bull. Amer. Meteor. Soc.*, **95**, 1235–1248, doi:10.1175/BAMS-D-13-00043.1.

Dirmeyer, P. A., X. Gao, and T. Oki, 2002: The Second Global Soil Wetness Project (GSWP2). International GEWEX Project Office Publication, IGPO Publication Series, No. 37, 65 pp.

Dudhia, J., 1989: Numerical study of convection observed during the Winter Monsoon Experiment using a mesoscale two-dimensional model. *J. Atmos. Sci.*, **46**, 3077–3107, doi:10.1175/1520-0469(1989)046<3077:NSOCOD>2.0.CO;2.

Entekhabi, D., and Coauthors, 2010: The Soil Moisture Active and Passive (SMAP) Mission. *Proc. IEEE*, **98**, 704–716, doi:10.1109/JPROC.2010.2043918.

Fernando, H. J., and Coauthors, 2015: The MATERHORN: Unraveling the intricacies of mountain weather. *Bull. Amer. Meteor. Soc.*, **96**, 1945–1967, doi:10.1175/BAMS-D-13-00131.1.

Fry, J., and Coauthors, 2011: Completion of the 2006 national land cover database for the conterminous United States. *Photogramm. Eng. Remote Sens.*, **77**, 858–864.

García-Díez, M., J. Fernández, L. Fita, and C. Yagüe, 2013: Seasonal dependence of WRF model biases and sensitivity to PBL schemes over Europe. *Quart. J. Roy. Meteor. Soc.*, **139**, 501–514, doi:10.1002/qj.1976.

Hanna, S. R., and R.Yang, 2001: Evaluations of mesoscale models' simulations of near-surface winds, temperature gradients, and mixing depths. *J. Appl. Meteor.*, **40**, 1095–1104, doi:10.1175/1520-0450(2001)040<1095:EOMMSO>2.0.CO;2

Hart, K. A., W. J. Steenburgh, and D. J. Onton, 2005: Model forecast improvements with decreased horizontal grid spacing over finescale intermountain orography during the 2002 Olympic Winter Games. *Wea. Forecasting*, **20**, 558–576, doi:10.1175/WAF865.1.

Holt, T. R., D. Niyogi, F. Chen, K. Manning, M. A. LeMone, and A. Qureshi, 2006: Effect of land–atmosphere interactions on the IHOP 24–25 May 2002 convection case. *Mon. Wea. Rev.*, **134**, 113–133, doi:10.1175/MWR3057.1.

Hong, S. Y., Y. Noh, and J. Dudhia, 2006: A new vertical diffusion package with an explicit treatment of entrainment processes. *Mon. Wea. Rev.*, **134**, 2318–2341, doi:10.1175/MWR3199.1.

Horel, J., and Coauthors, 2002: MesoWest: Cooperative mesonets in the western United States. *Bull. Amer. Meteor. Soc.*, **83**, 211–225, doi:10.1175/1520-0477(2002)083<0211:MCMITW>2.3.CO;2.

Hu, X. M., P. M. Klein, and M. Xue, 2013: Evaluation of the updated YSU planetary boundary layer scheme within WRF for wind resource and air quality assessments. *J. Geophys. Res.*, **118**, 10 490–10 505, doi:10.1002/jgrd.50823.

Huang, J., H. M. van den Dool, and K. P. Georgarakos, 1996: Analysis of model-calculated soil moisture over the United States (1931–1993) and applications to long-range temperature forecasts. *J. Climate*, **9**, 1350–1362, doi:10.1175/1520-0442(1996)009<1350:AOMCSM>2.0.CO;2.

Iacono, M. J., J. S. Delamere, E. J. Mlawer, M. W. Shepard, S. A. Clough, and W. D. Collins, 2008: Radiative forcing by long-lived greenhouse gases: Calculations with the AER radiative transfer models. *J. Geophys. Res.*, **113**, D13103, doi:10.1029/2008JD009944.

Jackson, T. J., and Coauthors, 2010: Validation of Advanced Microwave Scanning Radiometer soil moisture products. *IEEE Trans. Geosci. Remote Sens.*, **48**, 4256–4272, doi:10.1109/TGRS.2010.2051035.

Kain, J. S., 2004: The Kain–Fritsch convective parameterization: An update. *J. Appl. Meteor.*, **43**, 170–181, doi:10.1175/1520-0450(2004)043<0170:TKCPAU>2.0.CO;2.

Kerr, Y. H., and Coauthors, 2010: The SMOS mission: New tool for monitoring key elements of the global water cycle. *Proc. IEEE*, **98**, 666–687, doi:10.1109/JPROC.2010.2043032.

Knievel, J. C., G. H. Bryan, and J. P. Hacker, 2007: Explicit diffusion in the WRF Model. *Mon. Wea. Rev.*, **135**, 3808–3824, doi:10.1175/2007MWR2100.1.

Larson, K. M., E. E. Small, E. Gutmann, A. Bilich, J. Braun, and V. Zavorotny, 2008: Use of GPS receivers as a soil moisture network for water cycle studies. *Geophys. Res. Lett.*, **35**, L24405, doi:10.1029/2008GL036013.

Lin, Y.-L., R. D. Farley, and H. D. Orville, 1983: Bulk parameterization of the snow field in a cloud model. *J. Climate Appl. Meteor.*, **22**, 1065–1092, doi:10.1175/1520-0450(1983)022<1065:BPOTSF>2.0.CO;2.

Liu, Y., and Coauthors, 2008a: The operational mesogamma-scale analysis and forecast system of the U.S. Army Test and Evaluation Command. Part I: Overview of the modeling system, the forecast products, and how the products are used. *J. Appl. Meteor. Climatol.*, **47**, 1077–1092, doi:10.1175/2007JAMC1653.1.

——, and Coauthors, 2008b: The operational mesogamma-scale analysis and forecast system of the U.S. Army Test and Evaluation Command. Part II: Interrange comparison of the accuracy of model analyses and forecasts. *J. Appl. Meteor. Climatol.*, **47**, 1093–1104, doi:10.1175/2007JAMC1654.1.

Marshall, C. H., K. C. Crawford, K. E. Mitchell, and D. J. Stensrud, 2003: The impact of the land surface physics in the operational NCEP Eta Model on simulating the diurnal cycle: Evaluation and testing using Oklahoma mesonet data. *Wea. Forecasting*, **18**, 748–768, doi:10.1175/1520-0434(2003)018<0748:TIOTLS>2.0.CO;2.

Mass, C. F., D. Ovens, K. Westrick, and B. A. Colle, 2002: Does increasing horizontal resolution produce more skillful forecasts? The results of two years of real-time numerical weather prediction over the Pacific Northwest. *Bull. Amer. Meteor. Soc.*, **83**, 407–430, doi:10.1175/1520-0477(2002)083<0407:DIHRPM>2.3.CO;2.

Massey, J. D., W. J. Steenburgh, S. W. Hoch, and J. C. Knievel, 2014: Sensitivity of near-surface temperature forecasts to soil properties over a sparsely vegetated dryland region. *J. Appl. Meteor. Climatol.*, **53**, 1976–1995, doi:10.1175/JAMC-D-13-0362.1.

McCumber, M. C., and R. A. Pielke, 1981: Simulation of the effects of surface fluxes of heat and moisture in a mesoscale numerical model. *J. Geophys. Res.*, **86**, 9929–9938, doi:10.1029/JC086iC10p09929.

Mellor, G. L., and T. Yamada, 1982: Development of a turbulence closure model for geophysical fluid problems. *Rev. Geophys. Space Phys.*, **20**, 851–875, doi:10.1029/RG020i004p00851.

Mlawer, E. J., S. J. Taubman, P. D. Brown, M. J. Iacono, and S. A. Clough, 1997: Radiative transfer for inhomogeneous atmospheres: RRTM, a validated correlated-*k* model for the longwave. *J. Geophys. Res.*, **102**, 16 663–16 682, doi:10.1029/97JD00237.

Nakanishi, M., and H. Niino, 2004: An improved Mellor–Yamada level-3 model with condensation physics: Its design and verification. *Bound.-Layer Meteor.*, **112**, 1–31, doi:10.1023/B:BOUN.0000020164.04146.98.

Ochsner, T. E., and Coauthors, 2013: State of the art in large-scale soil moisture monitoring. *Soil. Sci. Soc. Amer. J.*, **77**, 1888–1919, doi:10.2136/sssaj2013.03.0093.

Pleim, J. E., 2007: A combined local and nonlocal closure model for the atmospheric boundary layer. Part I: Model description and testing. *J. Appl. Meteor. Climatol.*, **46**, 1383–1395, doi:10.1175/JAM2539.1.

Reda, I., and A. Andreas, 2004: Solar position algorithm for solar radiation applications. *Sol. Energy*, **76**, 577–589, doi:10.1016/j.solener.2003.12.003.

Rife, D. L., T. T. Warner, F. Chen, and E. G. Astling, 2002: Mechanisms for diurnal boundary layer circulations in the Great Basin Desert. *Mon. Wea. Rev.*, **130**, 921–938, doi:10.1175/1520-0493(2002)130<0921:MFDBLC>2.0.CO;2.

Rodriguez-Alvarez, N., X. Bosch-Lluis, A. Camps, M. Vall-Ilossera, E. Valencia, J. F. Marchan-Hernandez, and I. Ramos-Perez, 2009: Soil moisture retrieval using GNSS-R techniques: Experimental results over a bare soil field. *IEEE Trans. Geosci. Remote Sens.*, **47**, 3616–3624, doi:10.1109/TGRS.2009.2030672.

Rostkier-Edelstein, D., and J. P. Hacker, 2010: The roles of surface-observation ensemble assimilation and model complexity for nowcasting of PBL profiles: A factor separation analysis. *Wea. Forecasting*, **25**, 1670–1690, doi:10.1175/2010WAF2222435.1.

Schaefer, G. L., M. H. Cosh, and T. J. Jackson, 2007: The USDA natural resources conservation service Soil Climate Analysis Network (SCAN). *J. Atmos. Oceanic Technol.*, **24**, 2073–2077, doi:10.1175/2007JTECHA930.1.

Seyfried, M. S., L. E. Grant, E. Du, and K. Humes, 2005: Dielectric loss and calibration of the Hydra Probe soil water sensor. *Vadose Zone J.*, **4**, 1070–1079, doi:10.2136/vzj2004.0148.

Steenburgh, W. J., S. F. Halvorson, and D. J. Onton, 2000: Climatology of lake-effect snowstorms of the Great Salt Lake. *Mon. Wea. Rev.*, **128**, 709–727, doi:10.1175/1520-0493(2000)128<0709:COLESO>2.0.CO;2.

Sukoriansky, S., B. Galperin, and V. Perov, 2005: Application of a new spectral theory of stably stratified turbulence to atmospheric boundary layers over sea ice. *Bound.-Layer Meteor.*, **117**, 231–257, doi:10.1007/s10546-004-6848-4.

Sun, W. Y., and M. G. Bosilovich, 1996: Planetary boundary layer and surface layer sensitivity to land surface parameters. *Bound.-Layer Meteor.*, **77**, 353–378, doi:10.1007/BF00123532.

Thompson, G., R. M. Rasmussen, and K. Manning, 2004: Explicit forecasts of winter precipitation using an improved bulk microphysics scheme. Part I: Description and sensitivity analysis. *Mon. Wea. Rev.*, **132**, 519–542, doi:10.1175/1520-0493(2004)132<0519:EFOWPU>2.0.CO;2.

Trier, S. B., F. Chen, K. W. Manning, M. A. LeMone, and C. A. Davis, 2008: Sensitivity of the PBL and precipitation in 12-day simulations of warm-season convection using different land surface models and soil wetness conditions. *Mon. Wea. Rev.*, **136**, 2321–2343, doi:10.1175/2007MWR2289.1.

WRCC, 2015: Western historical climate summaries: Dugway, Utah. Western Region Climate Center. [Available online at http://www.wrcc.dri.edu/cgi-bin/cliMAIN.pl?ut2257.]

Wyszogrodzki, A. A., Y. Liu, N. Jacobs, P. Childs, Y. Zhang, G. Roux, and T. T. Warner, 2013: Analysis of the surface temperature and wind forecast errors of the NCAR-AirDat operational CONUS 4-km WRF forecasting system. *Meteor. Atmos. Phys.*, **122**, 125–143, doi:10.1007/s00703-013-0281-5.

Zeng, X., Z. Wang, and A. Wang, 2012: Surface skin temperature and the interplay between sensible and ground heat fluxes over arid regions. *J. Hydrometeor.*, **13**, 1359–1370, doi:10.1175/JHM-D-11-0117.1.

Zhang, H., Z. Pu, and X. Zhang, 2013: Examination of errors in near-surface temperature and wind from WRF numerical simulations in regions of complex terrain. *Wea. Forecasting*, **28**, 893–914, doi:10.1175/WAF-D-12-00109.1.

Zheng, W., H. Wei, Z. Wang, X. Zeng, J. Meng, M. Ek, K. Mitchell, and J. Derber, 2012: Improvement of daytime land surface skin temperature over arid regions in the NCEP GFS model and its impact on satellite data assimilation. *J. Geophys. Res.*, **117**, D06117, doi:10.1029/2011JD015901.

Zhong, S., and J. Fast, 2003: An evaluation of the MM5, RAMS, and Meso-Eta models at subkilometer resolution using VTMX field campaign data in the Salt Lake valley. *Mon. Wea. Rev.*, **131**, 1301–1322, doi:10.1175/1520-0493(2003)131<1301:AEOTMR>2.0.CO;2.

Zhou, X., and B. Geerts, 2013: The influence of soil moisture on the planetary boundary layer and on cumulus convection over an isolated mountain. Part I: Observations. *Mon. Wea. Rev.*, **141**, 1061–1078, doi:10.1175/MWR-D-12-00150.1.

Zilitinkevich, S., 1995: Non-local turbulent transport: Pollution dispersion aspects of coherent structure of convective flows. *Air Pollution Theory and Simulation, Air Pollution III*, H. Power, N. Moussiopoulos, and C. A. Brebbia, Eds., Vol. I, Computational Mechanics Publications, 53–60.